Investigation of Pressure Fluctuations caused by Turbulent and Cavitating Flow around a P1356 Ship Propeller

Conxita Lifante, Thomas Frank

ANSYS Germany GmbH, Otterfing, Germany

Karsten Rieck

Schiffsbau-Versuchsanstalt GmbH, Potsdam, Germany

Summary:

The onset of cavitation around propellers, hydrofoils, ships, etc represents an important issue in terms of reduced performance, erosion and passenger/crew comfort due to cavitation induced vibrations and noise among other drawbacks. Consequently cavitation has been studied by many researchers, but up to now most of the investigations are still experiments. Since experimental investigations for marine applications are expensive, CFD simulations represent a powerful tool in order to investigate the phenomenon and consequently to improve the design of such components.
The final goal of this work is to get a deeper understanding of the structure of the flow around a propeller of a passenger ship. The accurate prediction of cavitation has been found out to be intrinsically related to the accurate resolution of turbulent structures of the flow. Therefore, a thoroughly analysis of the turbulence modeling in this kind of application was performed.
Two cases have been analyzed. The first one is a 3D case, where the fluid flows around a NACA 66_2-415 hydrofoil. A tip vortex is generated with high radial velocity gradients originating cavitation. This testcase offers some simplification with respect to the P1356 propeller flow due to the simpler shape of the hydrofoil and the stationary hydrofoil geometry incontrary to the ship propeller rotation. Therefore it can be regarded as an appropriate first approach to the study of the flow around the propeller and formation of turbulence/vortex induced cavitation. The second case is the flow around the P1356 propeller itself. In both cases the simulations have been carried out following the Best Practice Guidelines (BPG), and different grids and turbulence models have been investigated. The numerical results obtained have been compared to the experimental data available in literature for the first case, and to experimental data generated at SVA Potsdam, which includes transient pressure signals as well as cavitation patterns, for the second case. A highly satisfactory agreement between numerical solutions and experiments is observed for both test cases.

Keywords:

Cavitation, CFD, turbulence, DES, marine applications

1 Introduction

Cavitation in marine applications like flows around ships and propellers is a phenomenon, which can lead to serious performance deterioration of propellers, to damages to their blades and to loss of comfort due to the induced pressure fluctuations. Therefore large efforts are spent into the investigation of cavitation inception and accurate prediction of cavitation for existing and new marine technology designs. Due to high operational costs of experimental investigations it is highly desirable to be able to study cavitation with reliable CFD techniques.

The aim of this work is to investigate cavitation occurring at the propeller blades of a P1356 passenger ship. However, due to the high skewness of the propeller blades, and the complexity of the flow around it, a simpler case has been investigated first. It consists of a flow around a NACA 66_2-415 hydrofoil with elliptical planform, where the formation of a tip vortex can be observed. High radial velocity gradients lead to low pressure below saturation pressure in the vortex core inducing cavitation.

Different turbulence models have been applied and compared between them. The basic model considered was the two-equation model SST (Shear Stress Transport) [1][2]. In order to assess the minimum pressure in the trailing vortex core with strong swirling motion and high velocity gradients a curvature correction term [3][4] in the SST turbulence model was applied, leading to a substantial improvement in the accuracy of predicted fluid velocities. Further enhanced results were obtained by changing the turbulence model to a Reynolds Stress Model (RSM) [5]

For both testcases numerical simulations using ANSYS CFX have been performed on hierarchically refined meshes applying the Best Practice Guidelines by Menter [6]. Comparison of radial velocity profiles in the tip vortex showed good agreement with experimental data. Also it was found, that the mesh resolution of the finest mesh was still too coarse in order to fully resolve the very sharp velocity gradients in circumferential fluid velocities in the tip vortex close to the hydrofoil, when using the SST turbulence model. These investigations revealed the strong influence of the turbulence modeling on cavitation prediction, especially in the case of turbulence induced cavitation due to formation of recirculation zones or departing tip vortices.

After the analysis of the hydrofoil, the propeller case has been investigated. Experimental data provided by the Schiffsbau-Versuchsanstalt Potsdam GmbH (SVA) are used to validate the numerical simulations performed using ANSYS CFX. Among other facilities, SVA operates a towing tank and a cavitation tunnel. In the cavitation tunnel the P1356 propeller model was investigated with a plate located 18.2cm above the propeller and four pressure transducer probes on the plate. The plate with pressure transducers is representing the very simplified ship stern and the pressure sensors were used to record transient pressure signals in order to study the propeller/ship stern interaction in cavitating and not cavitating flow conditions.

Grid and turbulence modeling dependencies are found to play a crucial role in order to reproduce accurately the pressure field around the propeller, and furthermore in accurate prediction of vortex induced cavitation.

Different approaches are considered for the generation of the grid (by means of the ICEM CFD software) not only including regular spatial refinement but also the adequate location of nodes in the more essential zones of tip vortex cavitation by applying locally unstructured meshing techniques to selected blocks of a structured mesh in combination with a new technique for the rotor-stator interface around the propeller. Especially demanding is the resolution of the grid in locations, where the tip vortices depart from the blade tips of the propeller. Trailing vortices from blade tips represent comparable small spatial structures and their sufficient resolution in space is essential for the vortex representation in the CFD solution and for small numerical diffusion to the large pressure and velocity gradients in these vortex structures. The exact as possible prediction of the local pressure minima in the tip vortex cores is finally of essential importance for the prediction of vortex induced cavitation inception in these numerical simulations.

Different turbulence models are analyzed and compared to each other, starting from a transient two-equation approach by means of the SST model, EARSM, a k-ω-based RSM (all turbulence viscosity based URANS methods) and ending up with scale-adaptive simulation (SAS) [7] or detached eddy simulations (DES). The numerical results obtained show satisfactory agreement to the experimental

data, and the use of ANSYS CFX has proven to be an accurate and suitable tool to investigate the phenomena of tip vortex separation and cavitation inception on propeller blades in marine applications.

2 Test cases definition

The final goal of this work was the study of the passenger ship propeller P1356. However, since its geometry and configuration is specially complicated due to the skewness of propeller blades and the usage of a rotor-stator interface for the propeller rotation, a simpler test case was analyzed first: an elliptical planform hydrofoil, the so-called Arndt profile case. Experimental data is available in the literature [8][9], and the numerical results obtained have been compared to them. This case provides us with useful information and hints about how to approach the study of the propeller in terms of mesh resolution, numerical scheme parameters, suitable CFD setup and turbulence modelling.

2.1 Arndt case

A three dimensional case consisting of a flow around a NACA 66_2-415 hydrofoil with elliptical planform was investigated. In this case tip-vortex cavitation takes place due to the high radial velocity gradients in the vortex tube, which is released from the tip of the hydrofoil. Highly swirling flow generates pressure drop below saturation pressure leading to cavitation on the tip of the hydrofoil and in the vortex core of the tip-vortex.

2.1.1 Description

The test body used in the original facility consists of an elliptical planform hydrofoil with a chord length of 81mm, a semi span of 95mm and a mean line of 0.8. Figure 1 shows a representation of the experimental flow geometry which was exactly used for the CFD simulations as well.

In accordance with the original publication of Arndt an effective angle of attack has been defined as $\alpha_{eff} = \alpha - \alpha_0$, where α_0 corresponds to the zero lift angle, which after a parametric study was chosen as α_0=2.5°.

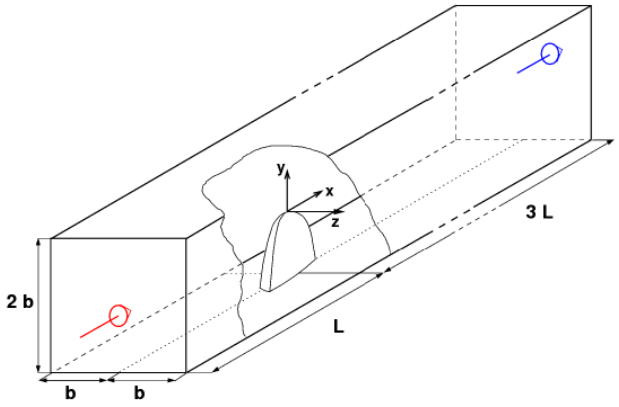

Figure 1: Schematic representation of the NACA 66_2-415 cavitation channel setup.

2.1.2 Numerical meshes

Following the Best Practice Guidelines, different grids were created for the numerical simulations. The ICEM CFD Hexa grid generator [10] has been used to discretise the domain. A block structure allowing to refine the grid near the blade surface as well as to perform a smooth transition between coarsely resolved areas in the far field and finely resolved areas around the hydrofoil was designed. The coarser mesh obtained with this block structure is presented in Figure 2. The designed grid block structure guarantees a minimum grid angle larger then 20° independent from the grid refinement level. As for the previous case a mesh refinement study has been carried out, employing three different grids, which are refined by a factor of $\sqrt[3]{4}$ in each coordinate direction. The same parameters were taken into account to evaluate the quality of the mesh: minimum angle formed by the grid lines, aspect ratios and the near wall distance of the first mesh element.

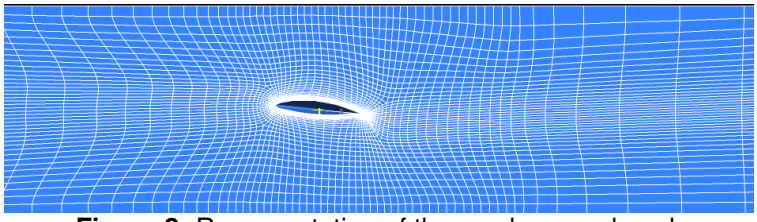

Figure 2: Representation of the meshes employed**.**

The main information related to the grid properties and grid quality on various mesh levels of refinement used to run the CFD simulations is summarized in Table 1.

	Nodes	**Min grid angle**	**Average y^+**
Coarse	358.519	20.9º	14.3
Medium	1.394.862	20.7º	7.1
Fine	5.442.459	20.1º	3.6

Table 1: Grid statistics

2.1.3 Numerical Setup

The simulations included in this work have been run in a transient mode using a multi-phase CFD setup with water and water vapor under normal conditions as the working fluids. The evaluation of the vapor volume fraction is based on the resolution of the Rayleigh-Plesset equation [11], which in its complete form is reading like

$$R_B \frac{d^2 R_B}{dt^2} + \frac{3}{2}\left(\frac{dR_B}{dt}\right)^2 + \frac{2\sigma}{\rho_l R_B} = \frac{P_v - P}{\rho_l} \tag{1}$$

where R_B represents the bubble radius, σ is the surface tension coefficient and P_v is the pressure in the bubble, which is assumed to be the vapor pressure.

A high resolution numerical scheme has been chosen for the advection term and a second order backward Euler scheme for the transient term.

The following boundary conditions were applied to solve the test case:

- Inlet boundary condition with an inlet velocity value based on the Reynolds number.

$$v_{in} = \frac{\mathrm{Re}\,\mu}{\rho L} \tag{2}$$

- Outlet boundary condition with a static outlet pressure based on the cavitation number.

$$p_{out} = p_v + \sigma_n \left(\frac{\rho}{2} v_{in}^2\right) \tag{3}$$

- No-slip wall boundary condition for the cavitation tunnel walls and the solids inside the domain. The CFX automated wall treatment has been applied for turbulence boundary conditions in dependency on y^+ values of the first mesh cell.

Different configurations were analyzed by changing the angle of attack, the Reynolds number characterizing the incident flow conditions and applying different turbulence modeling approaches: SST, SST with curvature correction term and BSL RSM. However, in this paper only results corresponding to a Reynolds number of Re=5.2x10^5, an effective angle of attack of α_0=12º and a cavitation number of σ_n=0.58 are presented. Their descriptions are summarized in Table 2.

Test name	Grid	Turbulence Model
1A	Coarse	SST
1B	Coarse	SST+High Res
1C	Coarse	SST+High Res+CC
1D	Coarse	BSL-RSM
2A	Medium	SST
2B	Medium	SST+High Res
2C	Medium	SST+High Res+CC
2D	Medium	BSL-RSM
3A	Fine	SST
3B	Fine	SST+High Res
3C	Fine	SST+High Res+CC

Table 2: Test cases investigated.

2.2 Propeller P1356

The test case analyzed is the flow around a passenger ship propeller called P1356. It has been investigated experimentally as well as numerically. Experiments were performed in the cavitation tunnel operated at SVA. And the experimental data obtained were afterwards used to validate the numerical simulations performed by using the ANSYS CFX software package.

2.2.1 Description

The propeller consists of 5 blades and has a diameter of D=0.25 m. The specific configuration presented here consists of a rotation frequency of n=28 s^{-1}, a propulsion coefficient of J=0.6 and the cavitation number of σ_n=1.816.

The propeller has been investigated inside the cavitation tunnel with a transducer plate located 18 cm above the propeller, where 4 different probes were arranged in a regular pattern on the surface of the plate in order to record transient pressure values at pressure sensor locations. The pressure transducer plate is used in this arrangement as a strongly simplified replacement of a real ship stern model in order to study the propeller/ship hull interaction by propeller and cavitation induced pressure fluctuations. Recorded transient pressure signals are then used for the validation of CFD simulation results. Therefore the same propeller configuration and geometry at the same scale was used for the numerical simulations. The inner cross section of the SVA Potsdam cavitation tunnel is 850x850 mm^2. A schematic representation of the propeller, the pressure transducer plate arrangement and the probe distribution is shown in Figure 3.

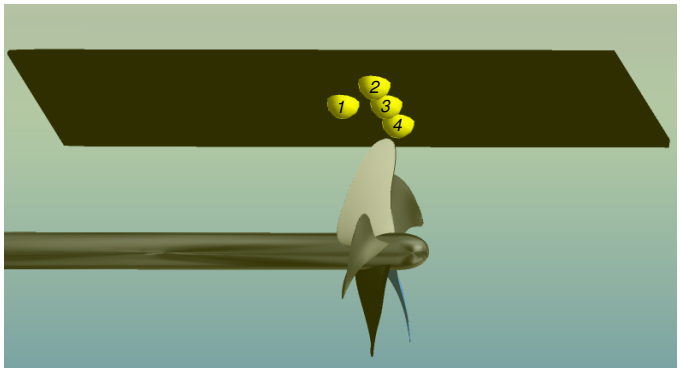

Figure 3: Test case configuration: propeller, transducer plate and probe locations.

The experimental data were generated after the propeller was rotating for long time, therefore assuring the independency of the recorded data from cavitation tunnel initial state. Then the signal corresponding to 10 cycles was recorded. For higher reliability of data, clearer plot representation and comparison to CFD results, a statistical average of the data over 10 propeller cycles was obtained.

2.2.2 Numerical meshes

The domain has been discretised using the mesh generator ANSYS ICEM-CFD [10].It has been split into two parts: one containing the area around the propeller blades (rotating region), and another one for the remaining static part of the domain. This is due to the fact that ANSYS CFX [12] allows running

different zones of the domain with either rotor or static frame of reference, and connecting them by using so-called general grid interfaces (GGI) at the rotor/stator interfaces.

In this way the propeller and a small part of the hub have been simulated in a rotor frame, while the rest of the domain (including the transducer plate) has been simulated in a static frame. As will be explained next, the spatial resolution of the grid at the interface between those two parts plays an important role in order to assure high accuracy of the numerical solutions.

Five different consequently refined grids were investigated (see Figure 4). The first approach (Grid1) contained about 1.4 Mio nodes in total. Due to the skewness of the propeller blades the minimum grid angle was about 9.25 degrees. Due to the generation of a scalable grid structure, this minimum grid angle could be preserved throughout the following steps of grid refinement, thereby assuring a constant mesh quality for all CFD predictions. The grid resolution at the rotor/stator interface in both domains was pointed out to be of quite significant influence on the CFD simulation results.

Therefore, the second step (Grid 2) consisted of refining the stator in order to get a more similar spatial resolution on both sides of the interface. Even with this approach the grid resolution of the static part of the computational domain was still rather coarse. Refining the grid at the stator domain in order to reach the same resolution as at the rotor side of the rotor/stator interface would imply a propagation of the refinement through the whole stator domain ending up with an enormous amount of nodes and consequently with a much too high computational effort for the computational flow prediction.

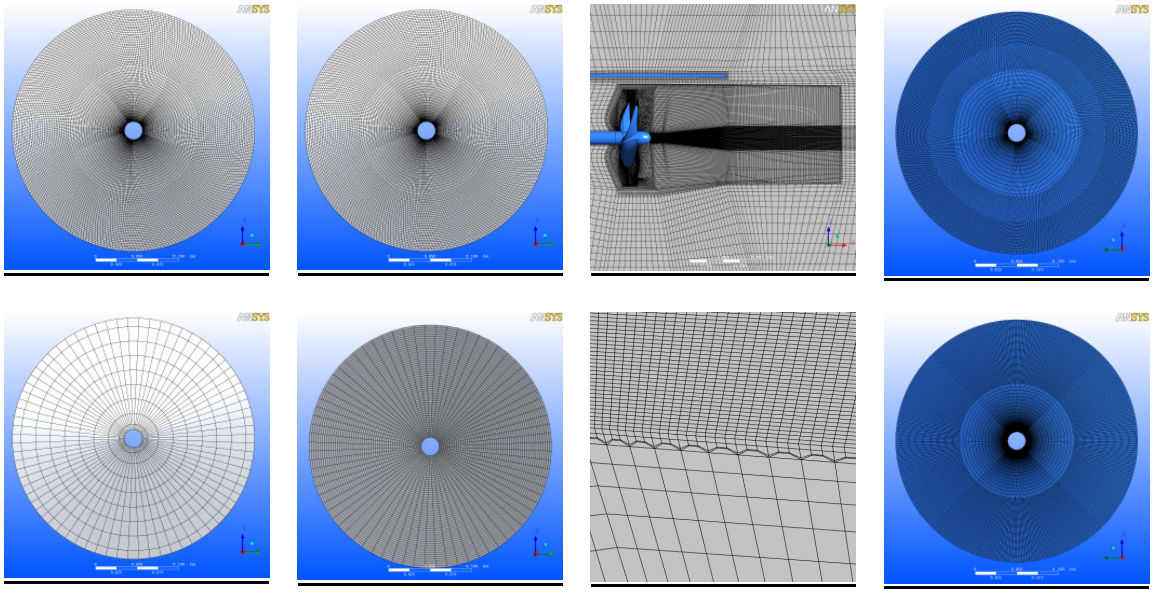

Figure 4: Grid resolution details for different meshes. From left to right: Grid 1 (rotor/stator interface); Grid 2 (rotor/stator interface), Grid 3 (structured/unstructured grid coarsening); Grid 5 (rotor/stator interface).

Therefore the third grid (Grid3) avoids this grid refinement propagation by applying a new feature of the ANSYS ICEM-CFD grid generator [13]. It allows generating a non-structured layer that creates a smooth transition between a densely refined zone of the grid and a coarser one (Figure 4). This way only a minor part of the stator (the one just after the interface, where the system of tip vortices is propagating downstream of the propeller) is refined, resulting in a similar spatial resolution on both sides of the rotor/stator interface.

The fourth mesh uses the same meshing strategy but nodes in the refined part of the stator domain are more concentrated in the area where the tip vortices departing from the blades are supposed to propagate. The final grid (Grid5) is a refinement of the previous one including an extension of the zone right after the interface where the grid is refined. The main characteristics of the grids used for the numerical simulations are summarized in Table 3.

	Nodes at rotor domain	Nodes at stator domain	Min grid angle
Grid1	1.159.050	270.460	9.25º
Grid2	1.159.050	605.620	9.25º
Grid3	1.159.050	3.117.222	9.25º
Grid4	1.196.825	3.847.814	9.00º
Grid5	1.627.550	8.464.877	9.90º

Table 3: Grid statistics

2.2.3 Numerical Setup

The simulations corresponding to the propeller case have been run in a transient mode using a single-phase CFD setup with water under normal conditions as the working fluid. A high resolution numerical scheme has been chosen for the advection term and a second order backward Euler scheme for the transient term.
The following boundary conditions were applied to solve the test case:

- Inlet boundary condition with an inlet velocity value based on the advance coefficient and rotation frequency.

$$v_{in} = JnD \tag{4}$$

- Outlet boundary condition with a static outlet pressure based on the cavitation number.

$$p_{out} = p_v + \sigma_n \left(\frac{\rho}{2} n^2 D^2 \right) \tag{5}$$

- No-slip wall boundary condition for the cavitation tunnel walls and the solids inside the domain. Again the CFX automated wall treatment has been applied for turbulence boundary conditions in dependency on y^+ values of the first mesh cell.

In order to investigate the influence of the two parameters (grid resolution, and turbulence modeling) different configurations were analyzed. Their description is summarized in Table 4. Besides the application of turbulence viscosity based URANS models, for the sufficiently refined numerical grids 3-5 also scale-resolving turbulence modeling (SAS-SST and DES) has been applied in the numerical simulations in order to reproduce the flow structure of detaching tip vortices correctly.

Test name	Grid	Turbulence Model
1A	1	SST
1B	1	SST+CC
1C	1	BSL-RSM
2A	2	SST
2B	2	SST+CC
2C	2	BSL-RSM
2D	2	EARSM
3A	3	SST
3B	3	SST+CC
3C	3	BSL-RSM
3D	3	EARSM
3E	3	SAS-SST
4E	4	SAS-SST
4F	4	DES
5F	5	DES

Table 4: Test cases investigated

3 Results

Two main characteristics or target properties have been analyzed in order to evaluate the results obtained with respect to the different grids and different turbulence models. For the hydrofoil case, these properties are the circumferential velocities in the tip vortex, and the water vapor isosurfaces

departing from the tip. The first ones can be compared to experimental values, while the second ones can be compared qualitatively to visual observations.

For the propeller case the information analyzed are the transient, ensemble averaged pressure signals at the probes located on the transducer plate and the tip vortex structure of the flow departing off the tips of the propeller blades and propagating downstream the cavitation tunnel behind the propeller. Again the first ones can be compared to recorded pressure data from the CFD simulations, while the second ones can be compared to visual observations and movies obtained directly from high-speed camera at the cavitation tunnel at SVA.

3.1 Arndt case

3.1.1 Velocity profile

In order to evaluate the quality of the obtained numerical results, the radial velocity profile at a location near the tip of the hydrofoil has been evaluated (one chord length far from it). A steep velocity gradient can there be observed. Further downstream dissipation of the tip vortex, a reduction in circumferential velocity amplitude as well as in velocity gradient could be observed.

The grid refinement allows to analyze the spatial discretization error of the numerical method and to evaluate if an asymptotical solution independent of the grid resolution can be finally obtained. For this purpose, the radial velocity profile was evaluated using the three refined grids and the SST turbulence modeling: case *1A/2A/3A* (
Figure 5). Small differences between the results can be observed even on the highest level of mesh refinement, indicating that a mesh independent solution could not yet be obtained. However, even more severe discrepancies to the experimental results arose, on measurement cross section further downstream the hydrofoil where the meshes are coarsening due to axial expansion.

A reason for this behavior is the strong swirl of the velocity field near the tip of the hydrofoil. In order to deal with this effect, different strategies have been considered. The first one consisted of the use of a High Resolution Scheme to solve the turbulence equations, which are solved by default using an upwind advection scheme, which is of cause more diffusive (case *3B*). But the influence of the chosen advection scheme, shown in Figure 6, was found to be not significant. In a second step a curvature correction term in the SST turbulence model had been applied (case *3C*), in order to account for the strong curvature of streamlines in the tip-vortex flow. The velocity profiles obtained with this curvature correction is also compared in Figure 6, showing an important improvement to approximate the strong velocity gradient.

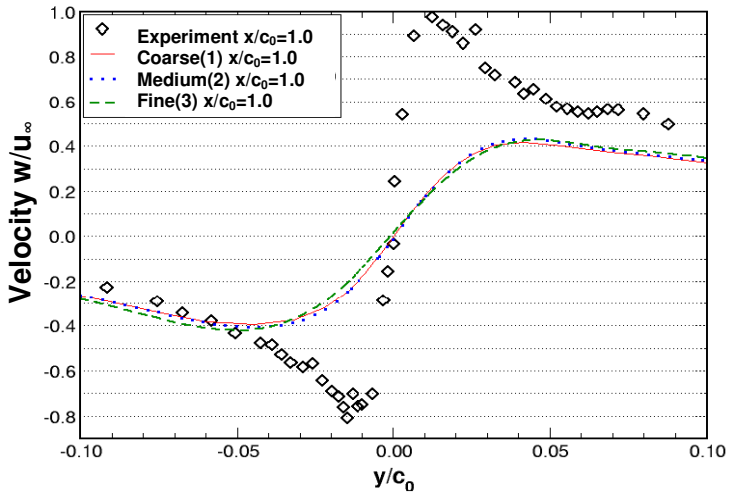

Figure 5: Radial velocity profiles for different grids at a chord length distance from the tip. SST model. Cases *1A/2A/3A*.

A further step was done in order to enhance the evaluation of the velocity gradient near the tip vortex by raising the limitation of assumed isotropic turbulence, which might be not satisfied in the strong swirling flow of the tip vortex behind the hydrofoil. Therefore the turbulence model was changed from a two-equation model to the BSL Reynolds Stress Model), where not two turbulence model equations but one equation for each Reynolds tensor component is solved. In this case (case *1D/2D*), the

computer and memory resources required has been increased, but analyzing Figure 6, it can be noticed that even for coarser meshes the enhancement is significant approaching in a more satisfactory comparison of the steep velocity profile to measurement data.

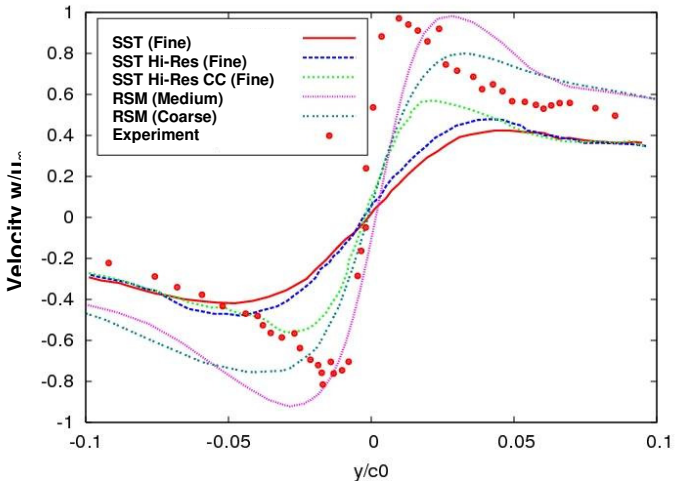

Figure 6: Radial velocity profile for different turbulence modeling. Cases *3A/3B/3C/1D/2D*.

3.1.2 Prediction of Tip Vortex Structure

The influence of the turbulence model can also be observed by looking into the vapor volume fraction obtained in an ANSYS CFX multiphase flow simulation applying the cavitation model in combination with SST and BSL RSM turbulence models. A larger tip vortex cavitation zone appears when the BSL Reynolds Stress Model is applied. Sheet cavitation is covering the most of the blade surface for both configurations (Figure 7).

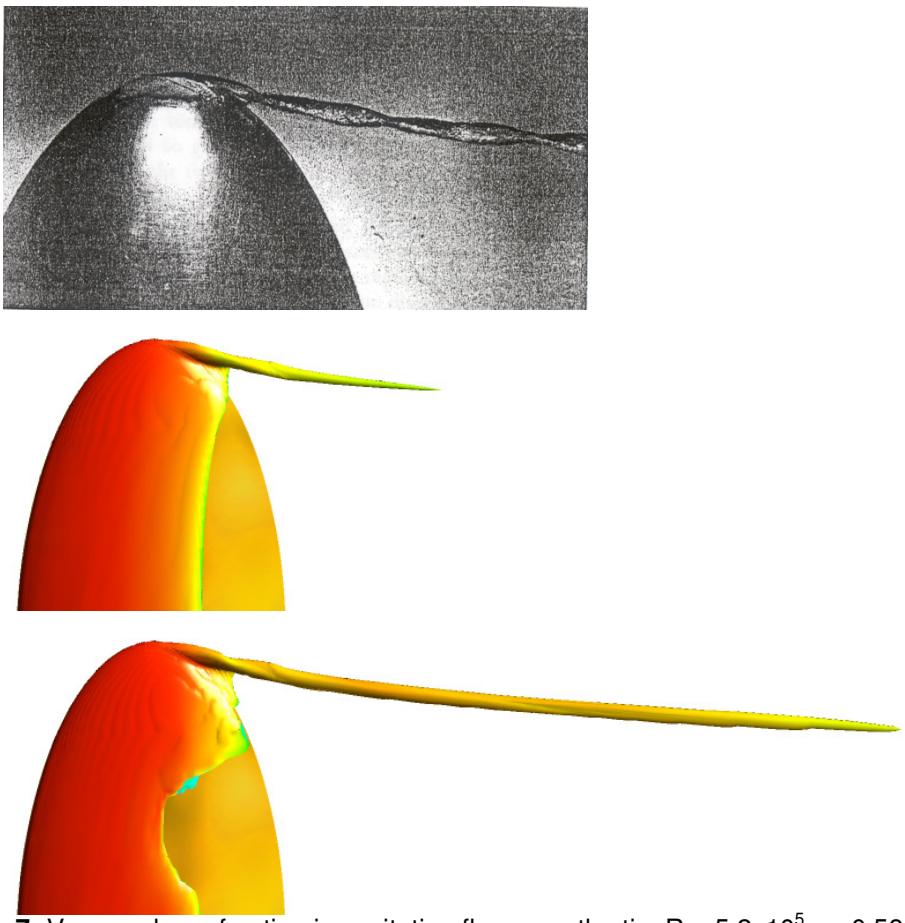

Figure 7: Vapor volume fraction in cavitating flow near the tip. Re=5.2x10^5. σ=0.58.. Top: experimental observation α_{eff}=9.5°; Middle: Case *3A*, α_{eff}=12°; Bottom: Case *2D*, α_{eff}=12°.

3.2 Propeller P1356

3.2.1 Transient Pressure Signals

The influence of the turbulence modeling can be observed in Figure 8. On its top, the transient pressure signal at the probe number 2 for the *1A/1B/1C* configurations is shown. Results show that for the Baseline Reynolds Stress Model approach the phase and the amplitude of the pressure signal is in better agreement with the experimental data then for the case using the standard SST w/o curvature correction, as could be expected, since it represents the more accurate turbulence model. The middle graphic contains the transient pressure signal for the *2B/2C/2D* configurations. In this case, the phase and amplitude prediction of the pressure signal is similar for the different models. There is no shift on the phase of the profiles, and the EARSM and the BSL-RSM show a very similar performance.

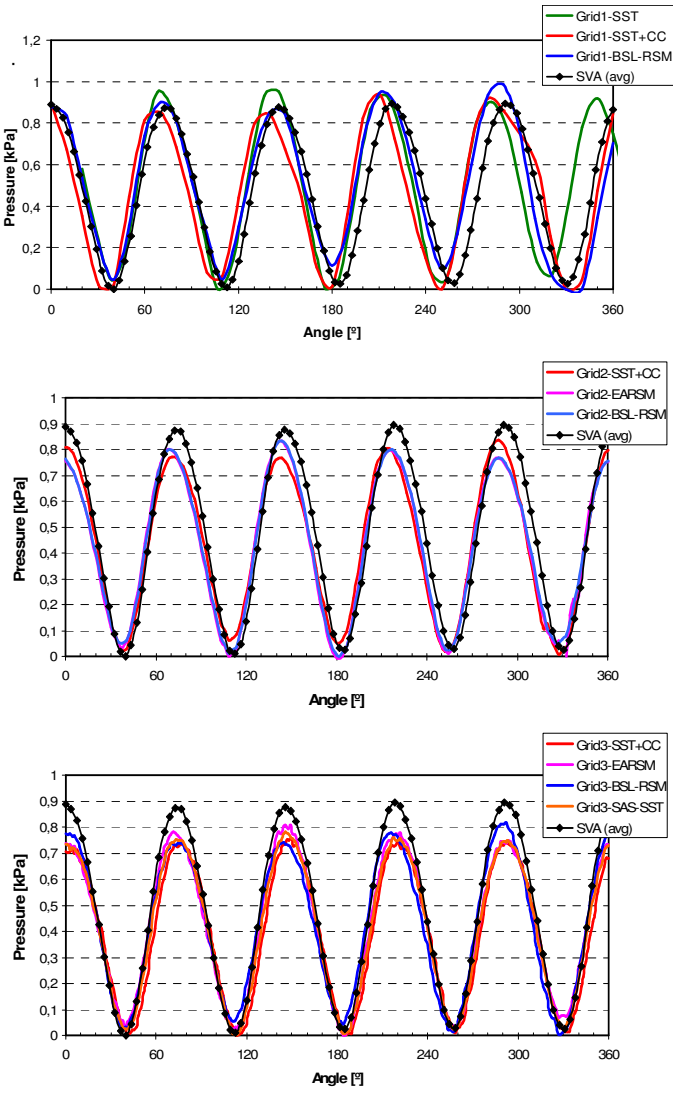

Figure 8: Transient pressure signal at probe 2 for different turbulence models. Top: Grid 1; Middle: Grid 2; Bottom: Grid 3

Results on the bottom correspond to the *3B/3C/3D/3E* simulations. The same qualitatively behavior can be observed. The influence of the grid resolution can be noticed in Figure 9. Results for the second probe, in this case for the simulations *3E/4F/5F*, are compared again to the experimental data. No significant difference between the fourth grid results and the third grid results is observed, as expected since the number of grid nodes is of the same order, grid resolution of the rotor domain is the same and only the location and number of nodes inside the rotor domain is changed. However, when the results on the 8.5 Mio nodes grid are analyzed (grid 5), it can be seen that the CFD simulations predict highly satisfactory the experimental results, even reaching the same amplitude level. The last grid contains more than twice the amount of nodes than the previous one.

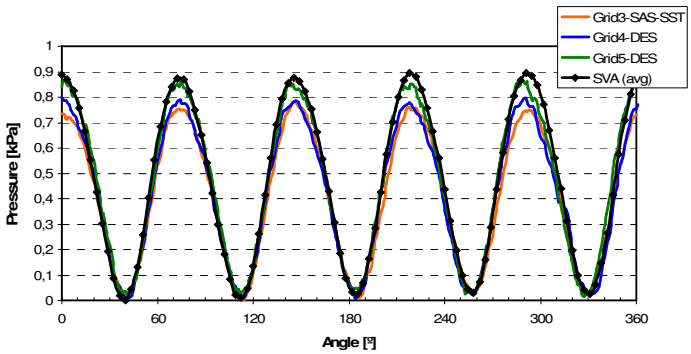

Figure 9: Transient pressure signal at probe 2. Cases *3E/4F/5F*.

3.2.2 Tip Vortex Structure

Since the final goal of the presented CFD study is the prediction of cavitation and the locations at the propeller blade surfaces where this will take place, the structure of the flow was investigated. Flow and vortex structure was analyzed more thoroughly by visualization of isosurfaces of the pressure field and turbulence related quantities.

In Figure 10 pressure isosurfaces for the five analyzed grids are plotted. Results correspond to the most accurate turbulence model in each case, so BSL RSM for grids 1-3 and DES for grids 4-5. The visualized domain includes the rotor including the propeller blades and the area in downstream direction. Black lines on the pictures represent the discretisation of the rotor/stator interface from the rotor point of view.

It was clearly found, that the first grid contained a too significant different resolution on both sides of the rotor/stator interface. Therefore a significant amount of information was lost at the rotor/stator interface due to interpolation errors. This can be noted because the tip vortices departing from the blades suddenly disappear on the interface location. The diffusion due to the interpolation between rotating and static parts of the computational domain does not allow them to cross the interface.

The second grid was refined in the circumferential direction in order to get a more similar spatial resolution on the mentioned interface. A slight improvement could be observed, because now the tip vortices cross the interface, but only a very short distance, almost insignificant. This indicated that the refinement was not still not sufficiently high, especially on the stator part of the domain adjacent downstream of the rotor domain. Thus, the necessity of a new meshing strategy arose.

The third grid simulation shows a notable progress in this sense. The isosurface length is larger, crossing the interface without loosing information. However, it looked not long enough as in the experimental facilities. In this case an optimization of the local node density was required, which was achieved by reallocation of nodes to the region, where the tip vortices propagate from the rotor domain into the stator domain keeping the overall number of nodes on the mesh almost constant.

The numerical results obtained with the fourth grid are more adequate in terms of tip vortices length prediction. The issue at the interface is totally fixed, and the characteristics of the results depend now on the global mesh parameters. However, some non-physical gaps in the lateral vortex structures appeared. This effect was not due to any deficiencies of the physical modeling but is related to the fact of non-appropriate projections of the edges of grid blocks in the far field behind the propeller. Larger cell sizes in the corners of rectangular grid block structures lead to a local coarsening of the numerical mesh with increasing distance to the rotor of the propeller and therefore to a deterioration in spatial resolution, which caused the tip vortices to disappear locally.

By fixing this meshing issue in grid 5 and by enlarging the area just behind the rotor/stator interface where the grid is refined, a very satisfactory result in agreement with the experimental observations was achieved. The pressure isosurfaces visualizing the location of the tip vortices show now a very comparable shape in comparison to the cavitation tunnel observations.

Since the resolution of the cavitation has an intrinsic relation with the degree of turbulence resolution, turbulence quantities can help us for the study and visualization of the flow structure. In this way, the so called Q-criteria value was analyzed. It is a velocity gradient invariant considering the vorticity and shear strain rate of the flow. It can be mathematically described as

$$Q = \Omega^2 - S^2 = \left(\frac{\partial u_i}{\partial x_j} - \frac{\partial u_j}{\partial x_i} \right)^2 - \left(\frac{\partial u_i}{\partial x_j} + \frac{\partial u_j}{\partial x_i} \right)^2 \qquad \textbf{(6)}$$

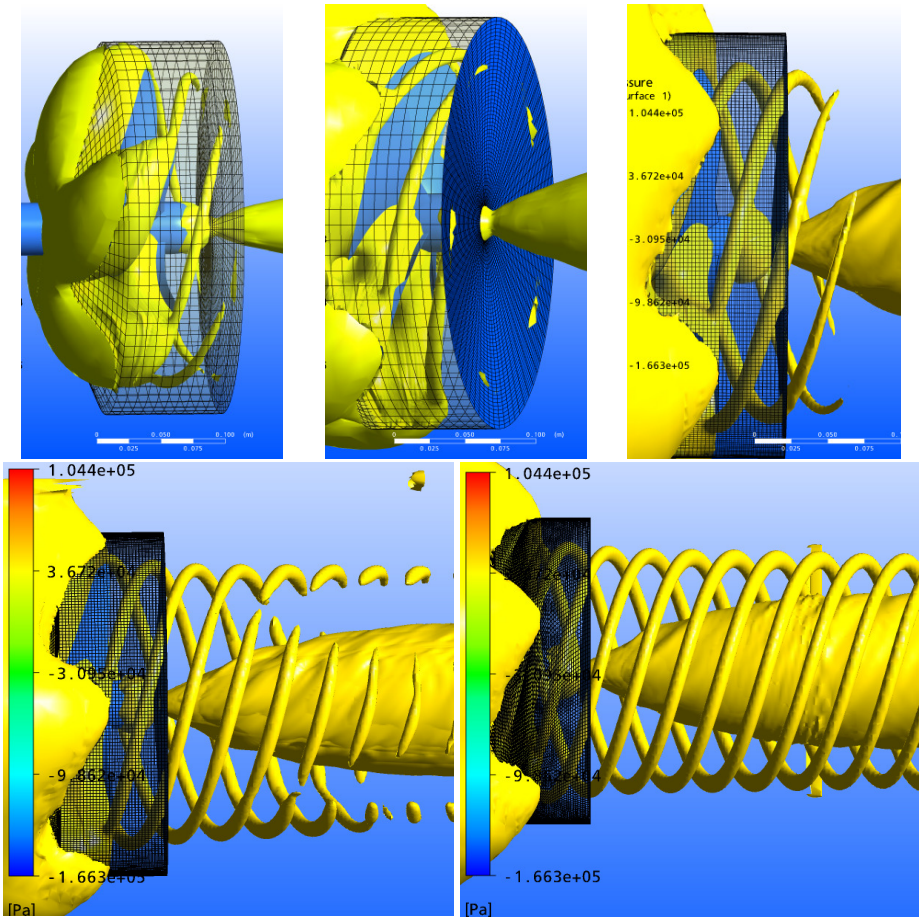

Figure 10: Pressure isosurface (P=47KPa) for the different grids. Top left: Case *1C*; Top middle: Case *2D*; Top right: *3F*; Bottom left: Case *4F*; Bottom right: Case *5F*.

This value has units of [s^{-2}]. In order to deal with a dimensionless parameter a modification of it was used. It has been done considering one of the more significant values characterizing the configuration of the flow, which is the rotation frequency of the propeller (*n*).

$$Q^* = Q/n^2 \tag{7}$$

In Figure 11 there is shown a qualitative comparison between a snapshot of the cavitation tunnel while the propeller is rotating (left) with the same parameters defined in the numerical simulations, and a plot of a Q^*-criteria isosurface obtained with the finest grid and using a DES model. It can be noted that the degree of agreement is fully satisfactory in terms of predicted flow structures behind the propeller.

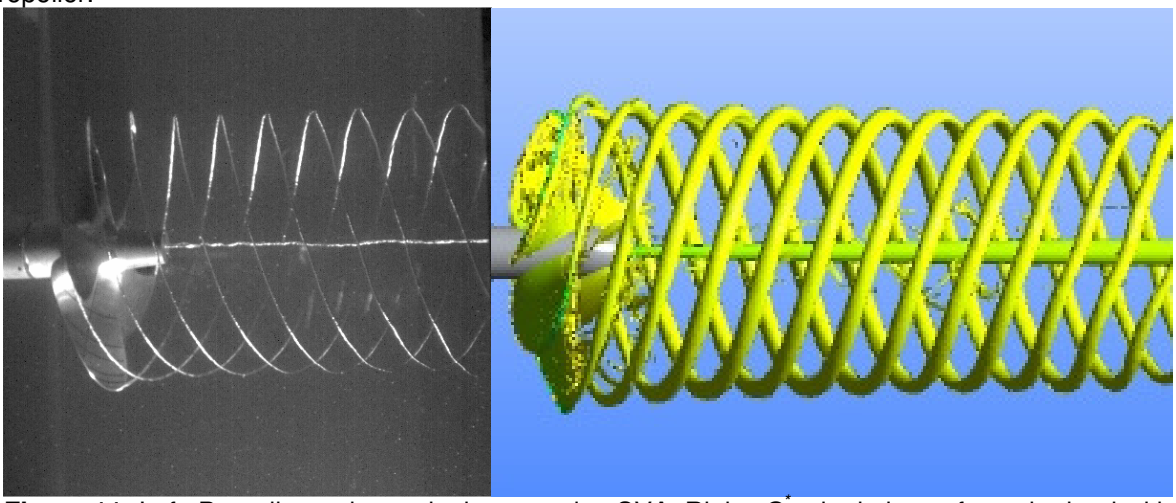

Figure 11: Left: Propeller at the cavitation tunnel at SVA; Right: Q^*-criteria isosurface obtained with numerical simulation. Case *5F* (Q^*=50).

4 Conclusions

The study of a flow around a hydrofoil and a ship propeller by means of CFD simulations was presented. This kind of flows are of large interest for the marine industry, and usually very costly when analyzed experimentally.

The main focus of the investigations in both cases was two-fold: to study the influence of grid resolution and turbulence modeling on transient pressure oscillations caused by the propeller/hydrofoil flow and on the flow structure downstream of it.

Therefore, different grids and turbulence models were considered. Both of them were found to have an important influence on the accuracy of the numerical solution, especially with respect to the spatial and timely resolution and downstream propagation of tip vortex structures departing from blade tips of the propeller.

The first test case is based on the experiments by Arndt. Special attention has been paid to the tip vortex, since this is the zone of the flow where larger velocity gradients appear as well as larger pressure drop occur, originating the inception of the tip-vortex cavitation. The trajectory of the tip vortex and the resolution of the radial velocities in the tip vortex have been investigated and compared to data. The velocity gradients were found to be difficult to compute and different strategies have been investigated. The basic simulations were run applying the standard SST turbulence model without any modifications, and it has been observed that the use of high order resolution schemes and the use of a curvature correction term improved the resolution of the steep velocity gradient near the tip of the hydrofoil. In addition, a Reynolds Stress Model has been applied showing a more satisfactory agreement to the numerical results even on coarser grids by taking into account the anisotropy of the continuous phase turbulence in the strong swirling flow in the tip vortex behind the tip of the hydrofoil.

For the propeller case, numerical results were compared to experimental data obtained from scaled model experiments at SVA Potsdam test facilities. With the finest grid and by applying a scale-resolving DES turbulence model very satisfactory agreement between numerical predictions and experiments could be observed, in terms of transient pressure signal predictions at given measurement locations and in terms of the predicted and visually observed flow structure behind the propeller blades.
The information obtained from the presented and discussed single-phase simulations indicate, that a multiphase simulation applying a cavitation model would require even finer grids in order to resolve the small geometrical structures of tip vortices and consequently the drop of the local pressure in tip vortices below the saturation pressure, which finally would lead to the turbulence induced tip vortex cavitation observable in the experiments.

5 Acknowledgments

Presented investigations have been supported by the German Ministry of Education and Research (BMBF) under grant number 03SX202A.

6 References

[1] Menter F., “Two-Equation Eddy-Viscosity Turbulence Models for Engineering Applications”, *AIAA Journal*, Vol. 32, No. 8, 1994, pp. 1598-1605.
[2] Menter, F.R., Rumsey, C.L., “Assessment of Two-Equation Turbulence Models for Transonic Flows”, *AIAA* 94-2343, Proc. 25th Fluid Dynamics Conference, Colorado Springs, Colorado, U.S.A., 1994.
[3] Langtry, R., Menter, F., “Transition Modeling for General Applications in Aeronautics”, *AIAA*, paper 2005-522, 2005.
[4] Spalart, P.R., Shur, M.L., „On the sensitization of turbulence models to rotation and curvature”, *Aerospace Science and Technology*, Vol. 1-5, S. 297-30, 1997.
[5] Wilcox, D.C., “Multiscale model for turbulent flows”, In *AIAA 24th Aerospace Sciences Meeting*. American Institute of Aeronautics and Astronautics, 1986.
[6] Menter F., “CFD Best Practice Guidelines for CFD Code Validation for Reactor Safety Applications”, ECORA Project, 2002, pp. 1-47.

[7] Menter, F. Egorov, Y., “A Scale-Adaptive Simulation Model using Two-Equation Models”, *AIAA Paper* 2005-1095, Reno/NV., 2005.
[8] Arndt, R.E.A., Dugue, C., “Recent Advances in Tip Vortex Cavitation Research”, Proc.The International Symposium on Propulsors and Cavitation, Hamburg, Deutschland, 22.-25. Juni, 1992.
[9] Arndt, R.E.A. and Arakeri , V.H., Higuchi, H., “Some observations of tip-vortex cavitation“, J. Fluid Mechanics, Vol. 229, 1991, pp. 269-289.
[10] ANSYS Inc., ICEM-CFD 12.0 “Users Manual”. 2007.
[11] Brennen, C.E., “Cavitation and Bubble Dynamics”. Oxford University Press. 1995.
[12] ANSYS Inc., ANSYS CFX 12.0 “Users Manual”, 2007.
[13] Schneiders, R., Schindler, R., Weiler, F., “Generation of Hexahedral Element Meshes”. *Proceedings of the 5th International Meshing Roundtable*, Pittsburgh, USA, 1996.